

HeTDSE: A GPU based program to solve full-dimensional-time-dependent Schrödinger equation for two-electron Helium subjected to strong laser fields

Xi Zhao*

Department of Physics, Kansas State University, Manhattan, KS 66506, USA

Electron-electron correlation plays an important role in the underlying dynamics in physics and chemistry. Helium is the simplest and most fundamental two-electron system. The dynamic process of helium in a strong laser field is still a challenging issue because of the large calculation cost. In this study, a GPU openACC based *ab initio* numerical simulations package HeTDSE is developed to solve the full dimensional time-dependent Schrödinger equation of helium subjected to a strong laser pulse. HeTDSE uses B-Spline basis sets expansion method to construct the radial part of the wavefunction, and the spherical harmonic functions is used to express for the angular part. Adams algorithm is employed for the time propagation. Our example shows HeTDSE running on an NVIDIA Kepler K20 GPU can outperform the one on an Intel E5-2640 single CPU core by a factor of 147. HeTDSE code package can got from the author or directly from the supplement materials of this work.

PACS numbers: 32.80.Rm, 42.50.Hz, 42.65.Ky

I. INTRODUCTION

The rapid development in laser technologies opens a way for scientists to probe and even control the fundamental dynamics of electron correlations [1–8]. As the simplest multi-electron atom, Helium is an idea starting point for exploring electron correlation dynamics in multi-electron systems [9–26]. However, due to its six degrees of freedom, the response of Helium to strong fields is considerably more complicated than that of single-electron atoms, which poses great theoretical and computational challenge. To overcome this difficulty, a set of conventional CPU parallel computing techniques have been developed to numerically solve the time-dependent Schrödinger equation (TDSE) of helium subjected to a laser pulse: Peng *et al.* investigated the electron correlation effects in two-photon-double-ionization (TPDI) of helium by finite-element-discrete-variable-representation (FEDVR) method [24]; Parker *et al.* used the finite-difference method to calculate the above threshold ionization (ATI) process [25]; Piraux *et al.* investigated the electron correlation effect by using the Gauss-Sturman function [14]. All of these simulations are very likely a numerical virtual experiment on the servers (about 200 to 1000 CPU cores are used in [24, 25]). Thus, more efficient algorithm is needed to further promoting the numerical simulations of Helium (and even more complex multi-electron systems beyond Helium) in strong laser fields investigations. One of this solution is Graphic Processing Unit(GPU) programming, which is the most powerful high performance computing tool so far and widely applied both in science and engineering numerically studies [27–34].

GPU contains hundreds of computing cores and is originally designed for the highly parallel process of graphic

rendering [27, 28]. Comparing with CPU, the computing performance of GPU can be increased by tens of times with proper optimizing [27–34]. To do this, a so-called "Compute Unified Device Architecture (CUDA)" GPU programming model is present [28]. However, porting of legacy CPU-based codes with CUDA often necessitates explicit compute and data management, thus requiring significant structural changes to existing applications [29]. Therefore, we make the choice to use OpenACC, which gives an alternative model as a GPU programming scheme [35]. OpenACC is a set of directive-based extensions to C, C++ and Fortran that allow programmers to annotate regions of code and data for offloading from a CPU host to an attached GPU, without requiring modification to the underlying CPU code itself. Programmers simply insert OpenACC directives before specific code sections to engage the GPU to accelerate the code. This approach enables the compiler to target and optimize parallelism automatically. More example programs and detailed description of openACC can be found in openACC official website [35].

In this work, we present a GPU based openACC fortran program HeTDSE, which is an efficient tool to investigate the non-perturbative electronic dynamics of helium subjected to a strong laser pulse by solving full-dimensional two-electron TDSE. It goes beyond the single-electron-approximation (SEA) approach and includes the response to the field of all two electrons. To build Helium wavefunction, B-Spline basis sets, which were widely used in computational atomic and molecular physics [36–47], are used to construct the radial part of the wavefunction, while the spherical harmonic functions is used to express for the angular part. The reason we use B-Spline basis sets to expand Helium radial wavefunction is that, B-Spline function has great advantages of describing both bound and continue states with small number basis sets [36, 37, 39]. Adams algorithm is employed for the time propagation [48]. Another advantage of using B-Spline basis sets and Adams method is that

*zhaoxi719@ksu.edu

it is easy to parallelize the code and will get an excellent parallel scaling with openACC.

The paper is organized as follows: In section 2, we present the theoretical background on HeTDSE. In Section 3 we exhibit an overview of the package structure, the input, output files and the code parallelizing. In Section 4 we show several test applications of HeTDSE. The parallel efficiency is given in Section 5. We present our conclusions in Section 6. Atomic units are used throughout, unless otherwise stated.

II. MATHEMATICAL SETUP AND ALGORITHM

A. B-Spline function

B-splines are functions designed to generalize polynomials for the purpose of approximating arbitrary functions, we use B-Spline basis sets to construct the Helium wavefunction in HeTDSE. Thus, we begin this Section with a brief description of B-Spline function, very details of B-Spline function can be found in ref [39].

A B-Spline function is defined by the order k and a set of the breakpoints $\{t_i\}$,

$$B_{j,1}(r) = \begin{cases} 1 & t_j \leq r \leq t_{j+1}, \\ 0 & \text{otherwise} \end{cases} \quad (1)$$

$$B_{j,k}(r) = \frac{r-t_j}{t_{j+k-1}-t_j} B_{j,k-1} + \frac{t_{j+k}-r}{t_{j+k}-t_{j+1}} B_{j+1,k-1},$$

The radial coordinates of Helium wavefunction is discrete in the interval $[r_{\min}, r_{\max}]$ by the breakpoints $\{t_j\}$. Three types of breakpoints sequence $\{t_j\}$ are used in HeTDSE [39]. The first one is linear sequence

$$t_i = r_{\min} + (r_{\max} - r_{\min}) \frac{i-1}{n-1}, \quad (2)$$

The sequence is divided into a equal length.

Second, exponential sequence,

$$t_i = r_{\min} + (r_{\max} - r_{\min}) \frac{e^{\gamma(\frac{i-1}{n-1})} - 1}{e^{\gamma} - 1} \quad i = 1, \dots, n, \quad (3)$$

This sequence tends to a linear sequence as $\gamma \rightarrow 0$ while all points exponentially accumulate close to r_{\min} as $\gamma \rightarrow \infty$.

Third, Linear-parabolic sequence. A useful sequence adapted to a good description of both the bound and the continuum states associate a linear spreading at large distances with a quadratic sequence close to the origin [39].

$$r_0 = \frac{r_{\max}(i_0 - 1) + r_{\min}(n - i_0)}{2n - i_0 - 1}$$

$$\alpha = \frac{r_0 - r_{\min}}{(i_0 - 1)^2}$$

$$\beta = \frac{r_{\max} - r_0}{n - i_0} \quad (4)$$

$$t_i = \begin{cases} r_{\min} + \alpha(i_0 - 1)^2 & 1 \leq i < i_0 \\ r_0 + \beta(i - i_0) & i_0 \leq i \leq n. \end{cases}$$

Other types sequences can be found in [39] and its references.

The derivative of a B-spline of order k can be expressed as a linear combination of B-Splines of the same order

$$\frac{dB_{j,k}(r)}{dr} = \frac{k-1}{t_{j+k-1} - t_i} B_{j,k-1}(r) - \frac{k-1}{t_{j+k} - t_i} B_{j+1,k-1}(r), \quad (5)$$

The B-Spline function order $k = 7$ is used throughout this work, so we don't write out k in B-Spline functions for simplification.

B. Time independent Schrödinger equation

The Helium eigenstate $\varphi_n(r_1, r_2)$ and its corresponding eigenvalue E_n is solution of time independent Schrödinger equation (TISE) of Helium:

$$H_0(r_1, r_2) \varphi_n(r_1, r_2) = E_n \varphi_n(r_1, r_2), \quad (6)$$

where $H_0(\mathbf{r}_1, \mathbf{r}_2)$ is the laser-free Hamiltonian

$$H_0(\mathbf{r}_1, \mathbf{r}_2) = -\frac{\nabla_1^2}{2} - \frac{\nabla_2^2}{2} - \frac{2}{r_1} - \frac{2}{r_2} - \frac{1}{|\mathbf{r}_1 - \mathbf{r}_2|}. \quad (7)$$

where $-\nabla_i^2/2 - 2/r_i$ with $i = 1, 2$ denotes the kinetic energy and potential energy of electron i , and $\frac{1}{|\mathbf{r}_1 - \mathbf{r}_2|}$ is the electron-electron correlation term. The time-independent Helium wavefunction is expanded as

$$\varphi_n(\mathbf{r}_1, \mathbf{r}_2) = \sum_{i=1}^N c_i [B_{n_1}(r_1) B_{n_2}(r_2) Y_{l_1 l_2}^{LM}(\hat{r}_1, \hat{r}_2) \quad (8)$$

$$+ (-1)^{l_1 + l_2 + L + S} B_{n_1}(r_2) B_{n_2}(r_1) Y_{l_1 l_2}^{LM}(\hat{r}_2, \hat{r}_1)]$$

where N is the number of the B-Spline basis sets for each time independent wavefunction $\varphi_n(r_1, r_2)$, l_1 (l_2) denotes the angular momenta for electron 1(2), L is the total orbital angular momentum, M is its z-component, S is the total spin, $\{c_i\}$ is the expansion coefficient and each i corresponds to a set of $\{n_1, l_1, n_2, l_2\}$. Coupled spherical harmonic functions is used to express for the angular part of the time-independent wavefunction:

$$Y_{l_1 l_2}^{LM} = \sum_{m_1 m_2} (-1)^{l_1 - l_2 + L} \sqrt{2L + 1} \begin{pmatrix} l_1 & l_2 & L \\ m_1 & m_2 & -M \end{pmatrix} \times Y_{l_1 m_1}(\hat{r}_1) Y_{l_2 m_2}(\hat{r}_2), \quad (9)$$

where $m_1(m_2)$ is the z-component of $l_1(l_2)$ and $Y_{lm}(\hat{r})$ is usual spherical harmonic functions.

The wavefunction $\varphi_n(r_1, r_2)$, eigenvalue E_n as well as the expansion coefficient $\{c_i\}$ in (8) can be got by directly diagonalizing eq. 6. For this purpose, there are a set of matrix integrals would be done: the kinetic energy integral matrix element:

$$K_{ij} = \int_{r_{\min}}^{r_{\max}} B_j(r) \frac{d^2}{dr^2} B_i(r) dr, \quad (10)$$

the potential energy integral matrix element:

$$P_{ij} = \int_{r_{\min}}^{r_{\max}} B_j(r) \frac{B_i(r)}{r} dr, \quad (11)$$

the overlap integral:

$$O_{ij} = \int_{r_{\min}}^{r_{\max}} B_j(r) B_i(r) dr, \quad (12)$$

and the coupling term integral:

$$C_{ij} = \int_{r_{\min}}^{r_{\max}} B_j(r_1) \frac{B_i(r_1)}{|\mathbf{r}_1 - \mathbf{r}_2|} dr_1, \quad (13)$$

K_{ij} , P_{ij} and O_{ij} are straightforward to discretize and calculated. However, the calculation of C_{ij} is different. To calculate C_{ij} we expand the electron-electron correlation term a truncated multipole series:

$$\frac{1}{|\mathbf{r}_1 - \mathbf{r}_2|} \approx \sum_l \sum_m \frac{4\pi}{2l+1} \frac{r_{<}^l}{r_{>}^{l+1}} Y_{lm}^*(\hat{r}_1) Y_{lm}(\hat{r}_2). \quad (14)$$

Thus, each of the terms are handled in a similar manner to the one-electron operators [37]. In HeTDSE, all the integrals are carried by Gauss-Lagrange integration method, which has been widely used in other works [26].

C. Time dependent Schrödinger equation

We solve the Helium TDSE within dipole approximation and length gauge. The full-dimension-TDSE of helium is

$$i \frac{\partial}{\partial t} \Psi(\mathbf{r}_1, \mathbf{r}_2, t) = H(\mathbf{r}_1, \mathbf{r}_2, t) \Psi(\mathbf{r}_1, \mathbf{r}_2, t), \quad (15)$$

where the total Hamiltonian of atom-laser system is

$$H(\mathbf{r}_1, \mathbf{r}_2, t) = H_0(\mathbf{r}_1, \mathbf{r}_2) + H_I(t), \quad (16)$$

The interaction Hamiltonian of the helium and laser pulse is

$$H_I(t) = (\mathbf{r}_1 + \mathbf{r}_2) \cdot \mathbf{e}(t) = -(\mathbf{r}_1 + \mathbf{r}_2) \cdot \partial \mathbf{A}(t) \partial t, \quad (17)$$

where the vector potential of the laser pulse is

$$\mathbf{A}(t) = \hat{\varepsilon} A_0 e f(t) \sin(\omega t + \phi) / \omega, \quad (18)$$

here $\hat{\varepsilon}$ is the laser polarization direction, ω and ϕ are the frequency and the carrier envelope phase, respectively. $f(t)$ is the temporal envelope.

The total time dependent wavefunction $\Psi(\mathbf{r}_1, \mathbf{r}_2, t)$ can be expanded in terms of the field-free atomic eigenfunctions

$$\Psi(\mathbf{r}_1, \mathbf{r}_2, t) = \sum_{s=1}^{N_{\text{total}}} a_s(t) e^{-iE_s t} \varphi_s(\mathbf{r}_1, \mathbf{r}_2), \quad (19)$$

Here N_{total} is the total number of the wavefunction $\varphi_n(r_1, r_2)$. Substituting equation 19 into 15, the TDSE is converted into a set of coupled partial differential equations,

$$\begin{aligned} i \frac{d}{dt} a_n(t) &= \sum_m a_m(t) e^{-iE_{mn} t} \\ &\times \langle \varphi_n(\mathbf{r}_1, \mathbf{r}_2) | (r_1 Y_{10}(\hat{r}_1) + r_2 Y_{10}(\hat{r}_2)) | \varphi_m(\mathbf{r}_1, \mathbf{r}_2) \rangle \frac{\partial \mathbf{A}(t)}{\partial t} \end{aligned} \quad (20)$$

which can be solved by the Adams method, details of this algorithm can be found in [48]. The energy difference $E_{mn} = E_m - E_n$ and the transition dipole element between $\langle \varphi_n(\mathbf{r}_1, \mathbf{r}_2) |$ and $|\varphi_m(\mathbf{r}_1, \mathbf{r}_2) \rangle$,

$$d_{nm} = \langle \varphi_n(\mathbf{r}_1, \mathbf{r}_2) | (r_1 Y_{10}(\hat{r}_1) + r_2 Y_{10}(\hat{r}_2)) | \varphi_m(\mathbf{r}_1, \mathbf{r}_2) \rangle \quad (21)$$

can be calculated from the solution of eq. 6.

D. Absorbing boundary

The absorbing layer is defined by using the radius $R = \sqrt{r_1^2 + r_2^2}$. Let r_{mask} be the radius where the absorbing layer starts. An absorbing layer between r_{mask} and r_{max} is used to smoothly bring down the wavefunction and to prevent the unphysical reflection from the boundary. The absorbing function has the following form:

$$A(R) = \begin{cases} 1 & R \leq r_{\text{mask}} \\ \cos^{\frac{1}{8}} \left(\frac{\pi(R-r_{\text{mask}})}{2(r_{\text{max}}-r_{\text{mask}})} \right) & r_{\text{mask}} \leq R \leq r_{\text{max}} \end{cases} \quad (22)$$

Although we use an absorbing to avoid the nonphysical reflecting, the simulation box still need to be set big enough so that the physical system is not perturbed by the absorbing boundaries. Thus, there are two interpretation of the ionization yield. First, we directly calculate the single (double) ionization yield by summing all the possibilities of the wavefunction with an eigenvalue larger than $-2.0(0.0)$:

$$Y(t) = \sum_i^{E_i \geq -2.0(0.0)} |c_i(t)|^2. \quad (23)$$

Alternative, the ionization probability is calculated as

$$Y(t) = 1 - \langle \Psi(\mathbf{r}_1, \mathbf{r}_2, t) | \Psi(\mathbf{r}_1, \mathbf{r}_2, t) \rangle. \quad (24)$$

III. DESCRIPTION OF THE PACKAGE

HeTDSE code package contains 9 fortran files and 4 input files. The fortran driver programs, functions, subroutines, input and output files are all introduced briefly in this section.

A. fortran program files

These fortran codes should be run one by one: Firstly, running **eigen-equation.f** to solve Eq. 6 to get wavefunction $\varphi_n(r_1, r_2)$, eigenvalue E_n as well as the expansion coefficient $\{c_i\}$; Then, with the output files of **eigen-equation.f**, running **dipole.f90** to get the transition dipoles element $\langle \varphi_n(\mathbf{r}_1, \mathbf{r}_2) | (r_1 Y_{10}(\hat{r}_1) + r_2 Y_{10}(\hat{r}_2)) | \varphi_m(\mathbf{r}_1, \mathbf{r}_2) \rangle$; Next, running **matrix.f90** to prepare input files for **tdse.f90**; Finally, running **tdse.f90** to solve the Eq. (20) to get the time-dependent wavefunction $\Psi(\mathbf{r}_1, \mathbf{r}_2, t)$.

There are other five fortran programs **order.f**, **rsg.f**, **wig.f**, **angl16.f90** and **SUBROUTINE.f90** in HeTDSE. These five programs are the "support codes", we **DO NOT** suggest the users to modulate them.

B. lower-level functions and subroutines

The lower-level functions and subroutines in this program are:

PREQUAN: Get the index of the one electron functions $B_n(r) Y_{lm}$ from 1 to $n \times (l_{\max} + 1)$.

QUAN2012: Select the basis sets that satisfies physics considerations: the one electron angular momenta l_1, l_2 should satisfy $|l_1 - l_2| \leq L \leq |l_1 + l_2|$ and the wavefunction $\Psi(r_1, r_2) \neq 0$.

gauleg: Calculate the Gauss-Lagrange integration.

DBSP2: Calculate second derivative of B-Spline function $d^2 B_n(r) / dr^2$.

DBSP1: Calculate first derivative of B-Spline function $dB_n(r) / dr$.

RKTSQ: Set the breakpoints distribution.

Bspline2006: Calculate the B-Spline function $B_n(r)$.

SingleInteg2012: Calculate the integration P_{ij}, K_{ij} or O_{ij} .

DmultiInteg2012: Calculate the electron-electron integration C_{ij} .

HAMILTON2012: Construct the Hamiltonian.

RSG: Diagonalize the matrix, get the energy level and wavefunctions.

ANG: Calculate the angle part of transition dipole element.

ode: Solve Eq. 20 by Adams algorithm.

f: Define the vector potential Eq. 18.

F3J0: Calculate 3-J symbol $\begin{pmatrix} j_1 & j_2 & j_3 \\ m_1 & m_2 & m_3 \end{pmatrix}$.

F6J: Calculate 6-J symbol $\begin{Bmatrix} j_1 & j_2 & j_3 \\ j_4 & j_5 & j_6 \end{Bmatrix}$.

abr: Set the absorbing boundary.

C. Input files

There are totally four input files in HeTDSE, **eigen-equation.input**, **dipole.input**, **matrix.input** and **tdse.input**,

which contain input parameters used by **eigen-equation.f**, **dipole.f90**, **matrix.f90** and **tdse.f90**, respectively. In this subsection, we will present how to set these parameters in these input files one by one.

eigen-equation.input

Line 1: Set total angular momentum L in Eq. 8.

Line 2: Set total spin in Eq. 8.

Line 3: Set max angular momentum for each electron l_{\max} .

Line 4: Set the order of the B-Spline function k .

Line 5: Set number of B-SPLINE function breakpoints, that is to say, n in Eq. 2, 3 and 4.

Line 6: Set total number of the basis sets for the He wavefunction N in Eq. 8.

Line 7: i_0 in Eq. (4).

Line 8: Set the simulation box size in radial direction, r_{\max} .

dipole.input

Line 1: Set total angular momentum L of $\langle \varphi_n(\mathbf{r}_1, \mathbf{r}_2) |$ and $|\varphi_m(\mathbf{r}_1, \mathbf{r}_2) \rangle$ in Eq. 8, respectively.

Line 2: Set total spin M of $\langle \varphi_n(\mathbf{r}_1, \mathbf{r}_2) |$ and $|\varphi_m(\mathbf{r}_1, \mathbf{r}_2) \rangle$ in Eq. 8, respectively.

Line 3 to Line 8 in **dipole.input** are the same with Line 3 to Line 8 in **eigen-equation.input**.

matrix.input

First value in Line 1, Line 2, Line 3 and Line 4: The number of the basis sets used in TDSE of states with $L = 0, L = 1, L = 2, L = 3$ and $L = 4$, respectively.

Second value in Line 1, Line 2, Line 3 and Line 4: The total number of the basis sets of states with $L = 0, L = 1, L = 2, L = 3$ and $L = 4$, respectively.

The default max total angular momentum is $L = 4$, larger total angular momentums can be added in this input file, if needed.

tdse.input

User should not change line 1 and line 2 in **tdse.input**, so we skip them and begin with Line 3.

Line 3: The maximum number of time steps allowed. Default value is 600 000.

Line 4: Frequency of the electric field in atomic unit.

Line 5: Number of the laser cycles.

Line 6: Intensity of the electronic laser field in atomic unit.

Line 7: Relative and absolute errors. Default values are 10^{-7} and 10^{-7} , respectively.

D. Output files

Output files of **eigen-equation.f**:

There are two output files after running **eigen-equation.f**: the coefficient c_i ($i = 1, \dots, N$) of the wavefunction $\varphi_n(r_1, r_2)$, and the eigenvalue E_n .

1. **S.dat** : This file stores the coefficient c_i in Eq.(6). The file name would change to **P.dat**, **D.dat**, **F.dat** and **G.dat** if $L = 1, 2, 3, 4$, respectively.

2. **OMEGA-S.dat**: This file stores the eigenvalue E_n of states with $\varphi_n(r_1, r_2)$. The file name would

change to *OMEGA-P.dat*, *OMEGA-D.dat*, *OMEGA-F.dat*, *OMEGA-G.dat* if $L = 1, 2, 3, 4$, respectively.

Output files of **dipole.f90**:

There is one output file after running **dipole.f90**: the transition dipole moment elements between a pair of states with neighbouring total angular momentums L and $L + 1$.

Output files of **matrix.f90**:

There are three output files after running *matrix.f90*:

1. *eigenval.out*: This file stores all the eigenvalues in the order $L = 0, 1, 2, 3, 4$.

2. *HI.dat*: This files stores all the dipole matrix elements.

3. *OMEGA.dat*: This files stores all the energy differences.

Output files of **tdse.f90**:

There are four output files after running **tdse.f90**:

1. *laser.dat*: This file stores laser field $E(t)$.

2. *single-ion.dat*: This file stores the single ionization yield $I_s(t)$.

3. *double-ion.dat*: This file stores the double ionization yield $I_d(t)$.

4. *c.dat*: This file stores the solution $a_n(t)$ ($n = 1, \dots, N_{total}$) of the coupled partial differential equations Eq. 20 at each time step. In principle, if we get $a_n(t)$, all the physical information can be retrieved.

E. OpenACC parallelizing implementation

In this subsection, we will explain the details of OpenACC implementation in HeTDSE. In HeTDSE package, more than 99% computation time would be paid to calculate transition dipole moment d_{mn} and time propagation. Thus, we will focus on accelerating the two calculations with openACC. In **dipole.f90** programs, four do-loops are needed to get all the transition dipole moment elements d_{mn} (see Eq. 21 for mathematical expression), and each loop would run 2000-10000 times. The code and corresponding openACC accelerated implementation is shown below:

```

1 !$ACC KERNELS
2   do m=1,NUMS
3     do n=1,NUMP
4       sum=0.d0
5       do i=1,NUMS
6         do j=1,NUMP
7           sum=sum+TERM(i,j)*c1(i,m)*c1p(j,n)
8         end do
9       end do
10      dipole(m,n)=sqrt(4.d0*pi/3.d0)*sum
11    end do
12  end do
13 !$ACC END KERNELS

```

although the computing scale is large, the code structure itself is really simple (nothing but a sum calculation)

and openACC can achieve a high performance parallelizing scaling. All four do-loops are parallelized directly by inserting the OpenACC directive `"$ACC KERNELS"`, then the data transfer between the host and the GPU memory is automatically executed. The calculation in the area (line 2 to line 12) of directive is executed and accelerated on GPU. Optimization for time propagation is similar, here is the Adams time propagation code at each time step and corresponding openACC accelerated implementation:

```

1 !$ACC PARALLEL LOOP PRIVATE(m,n)
2 do n=1,nhi
3   ap(n)=0
4   do m=1,nhi
5     ap(n)=ap(n)+sin(omega(n,m)-
6     &*t)*hi(n,m)*a(m)
7   end do
8   do m=nhi+1,neq
9     ap(n)=ap(n)+cos(omega(n,m-nhi)-
10    &*t)*hi(n,m-nhi)*a(m)
11   end do
12 end do
!$ACC END PARALLEL LOOP

```

As we known, the data transfer between the host and GPU memory affects the computational time. To further minimize the cost of data transfer, we use the OpenACC `"DATA COPY"` before time propagating starts, and `"END DATA"` is used to release the GPU memory at the end of time propagating:

```

1 !$ACC DATA COPY( hi,omega )
2 call ode(f,neq,a,t,&
3   &tout,relerr,abserr,iflag,work,iwork)
4 !$ACC END DATA

```

The datacopy (namelist) is the directive that copies the data from host to GPU memory, then data on GPU memory is used without the data transfer back and forth between the host and GPU every time step. Clearly, by inserting dotcopy, the calculational time is much saved.

The advantages of using B-Spline basis set and Adams method in HeTDSE are emphasized again at the end of this section: First, it is convenient to implement openACC. Second, the parallelizing scaling has a high performance, which will be shown in section 6.

IV. SAMPLE RESULTS

In order to verify the accuracy of our program, we compare our results with previous literatures. In the calculations, the radius of the cavity is $r_{1max} = r_{2max} = 70$ and it is described by 30 B-Spline functions of order 7. We use $l_{i=1,2} = 0, 1, 2, 3, 4$ and $L = 0, 1, 2, 3, 4$ in below simulation examples. Linear-parabolic breakpoints sequence is chosen. Total number of basis sets $N_{total} = 11000$ are used during the time dependent simulations.

A. ground and bound states calculation of Helium

In table 1, we show the eigenvalues of few low bound states for different total angular momenta. Table 1 shows that, for all the calculated levels, at least the accuracy up to two digits after the decimal point has been obtained. The density distributions of different atomic levels in coordinate space are shown in Fig. 1, where the results agree well with that in [23, 43, 44].

B. excited states dynamics

Now we turn to the second example: excited states dynamics. Here we focus on the carrier-envelope phase (CEP) effect on band-band state transition induced by a laser pulse. The CEP is a crucial parameter in describing the characteristics of a laser pulse, we can control the dynamic process of matter-laser interaction by measuring or adjusting the CEP [49–54]. Especially, the CEP effect on the bound-bound transition of an atom has been investigated both in theoretically and experimentally [49–54]. Here we try to reproduce the result from [52]. In [52], the authors used Hylleraas coordinates to reconstruct the wavefunction of Helium, and they introduced a parameter M to quantify the CEP effect:

$$M = \frac{P(\phi_{\max}) - P(\phi_{\min})}{[P(\phi_{\max}) + P(\phi_{\min})]^2}, \quad (25)$$

where $P(\phi_{\max})$ and $P(\phi_{\min})$ are, respectively, the maximum and minimum populations for a given excited state. A large value of M corresponding to a strong CEP effect. In this simulation, the laser parameters are the same as [52]. We use HeTDSE get the value M for 1D state after the laser ends, which is shown in Fig 2. Our result matches well with that in Fig.1(b) from [52].

C. excitation and ionization yields

Next, we calculate the excitation and ionization yields of helium in a strong laser pulse. Our basis sets covers the energy range located beyond the double-ionization threshold. The initial state is the ground state of Helium $|1S^2\rangle$. The laser pulse has a duration of 3.8 fs and the peak intensity of $2.97 \times 10^{14} \text{W/cm}^2$, which is the same as those in [38, 44]. Eq. 23. The present results in Fig. 3 are accordant with the data from Hasbani [38] and Scrinzi [44].

D. electrons wavepacket dynamics

We then calculate the electrons wavepacket dynamics both in coordinate space after the laser pulse. The frequency and FWHM of the laser pulse are $\omega = 1.0$ and 2 optical cycles, respectively, with the intensity of

$1.0 \times 10^{13} \text{W/cm}^2$. The continue state is collected as $\psi_{ion} = \sum_i c_i \varphi_i$, with $E_i > -2.0 \text{ a.u.}$

we get the wave function of helium at the end of the laser pulse. Using this wave function, the density distribution of the electrons in coordinate space can be obtained by

$$\rho(r_1, r_2, t) = \int \Psi(\mathbf{r}_1, \mathbf{r}_2, t) \Psi^*(\mathbf{r}_1, \mathbf{r}_2, t) r_1^2 r_2^2 d\Omega_1 d\Omega_2. \quad (26)$$

The density distribution of continuous states in coordinate space is shown in Fig. 4 when the laser is end. There is an evident single ionization characteristics in the figures, where the wave packet moves outside along the coordinate axis with time.

V. PARALLEL SCALING

To test the parallel efficiency of HeTDSE, we compare the serial CPU program (runs at Intel xeon E5-2640 CPU with 2.5GHz clock speed and 15MB L3 cache) and parallel GPU implementations (runs at NVIDIA K20 GPU with 2493 cores). The speedup factor for four simulation cases shown in Table II. The larger the basis number, the larger computation cost needs. All the simulations are done with PGI fortran compiler, the laser is 3.8 fs (which contains about 4000 time steps) and the simulation box is $R_{\max} = 70$. A speed up of 147 is achieved if 4300 basis sets are used. It indicates that as the simulation system size increases, this improvement becomes more and more pronounced.

VI. CONCLUSION

In this work, we present a program which solves the full-dimension-TDSE of helium using OpenACC+GPU simulation acceleration environment. We introduce how to convert the full-dimension-TDSE into coupled partial differential equations. These partial differential equations are solved by Adams method. Our program has two advantages: first, the codes are easily parallelled by adding few detectives and have a speed up of 147 on GPU, HeTDSE dose not have to use a super computer or a computer cluster, even a desktop computer with an openACC-enable GPU can run HeTDSE efficiently; second, we can transplant our program to other accelerators without rewriting the codes. By comparing with the literatures of the excited state dynamics and ionization yield of helium, the accuracy of our program has been verified. Our codes can be used to investigate the non-perturbative electronic dynamics of helium subjected to a strong laser pulse. Besides, for the programming for accelerators such as CUDA is difficult, we hope that HeTDSE to be an example to help more researchers to handle the GPU calculation more easily by using OpenACC.

VII. ACKNOWLEDGEMENTS

This research was supported in part by the Chemical Sciences, Geosciences, and Biosciences Division, Office

of Basic Energy Sciences, Office of Science, US Department of Energy, under Grant No. DE-FG02-86ER13491. XZ would also be supported by National Natural Science Foundation of China under Grant No. 11904192.

[1] T. Shintake *et al*, A compact free-electron laser for generating coherent radiation in the extreme ultraviolet region, *Nat. Photon.* **2** 555(2008).

[2] W. Ackermann *et al*, Operation of a free-electron laser from the extreme ultraviolet to the water window, *Nat. Photon.* **1** 336(2007).

[3] M. Hentschel, R. Kienberger, C. Spielmann, G. A. Reid, N. Milosevic, T. Brabec, P. Corkum, U. Heinzmann, M. Drescher, and F. Krausz, Attosecond metrology, *Nature* **414** 509(2001).

[4] P.M. Paul, E. S. Toma, P. Breger, G. Mullot, F. Augé, P. Balcou, H. G. Muller, and P. Agostini, Observation of a Train of Attosecond Pulses from High Harmonic Generation, *Science* **292** 1689 (2001).

[5] Chang-Long Xia, Xin-Lei Ge, Xi Zhao, Jing Guo and Xue-Shen Liu, Isolated attosecond pulse generation from a model of Ar cluster in a synthesized two-color laser pulse, *Phys. Rev. A* **85** 025802 (2012).

[6] Jing Guo, Xin-Lei Ge, Huiying Zhong, Xi Zhao, Meixia Zhang, Yuanfei Jiang and Xue-Shen Liu, Influence of vibrational states on high-order-harmonic generation and an isolated attosecond pulse from a N_2 molecule, *Phys. Rev. A* **90** 053410 (2014).

[7] Jun Zhang, Xue-Fei Pan, Xi Zhao, Jing Guo, Kai-Guang Zhu and Xue-Shen Liu, Spectral splitting and phase matching of the macroscopic high-order harmonic generation in intense laser fields, *J. Opt.* **21** 125503 (2019).

[8] Y. ZHAO, S. MA, S. JIANG, Y. YANG, X. ZHAO AND J. CHEN, All-optical reconstruction of k-dependent transition dipole moment by solid harmonic spectra from ultrashort laser pulses, *Opt. Express* **27** 34392 (2019).

[9] J. Colgan and M. S. Pindzola, Core-Excited Resonance Enhancement in the Two-Photon Complete Fragmentation of Helium, *Phys. Rev. Lett.* **88** 173002 (2002).

[10] L. Feng and H. W. van der Hart, Two-photon double ionization of He, *J. Phys. B* **36** L1 (2003).

[11] S. Laulan and H. Bachau, Correlation effects in two-photon single and double ionization of helium, *Phys. Rev. A* **68** 013409 (2003).

[12] B. Piraux, J. Bauer, S. Laulan, and H. Bachau, Probing electron-electron correlation with attosecond pulses, *Eur.Phys.J.D* **26** 7 (2003).

[13] S. X. Hu, J. Colgan, and L. A. Collins, Triple-differential cross-sections for two-photon double ionization of He near threshold, *J. Phys. B* **38** L35 (2005).

[14] E. Foumouo, G. L. Kamta, G. Edah, and B. Piraux, Theory of multiphoton single and double ionization of two-electron atomic systems driven by short-wavelength electric fields: An ab initio treatment, *Phys. Rev. A* **74** 063409 (2006).

[15] X. Guan, K. Bartschat, and B. I. Schneider, Dynamics of two-photon double ionization of helium in short intense xuv laser pulses, *Phys.Rev. A* **77** 043421(2008).

[16] T.Y. Shi and C. D. Lin, Double Photoionization and Transfer Ionization of He: Shakeoff Theory Revisited, *Phys. Rev. Lett.* **89** 163202(2002).

[17] H. Hasegawa, E. J. Takahashi, Y. Nabekawa, K. L. Ishikawa, and K. Midorikawa, Multiphoton ionization of He by using intense high-order harmonics in the soft-x-ray region, *Phys. Rev. A* **71** 023407 (2005).

[18] Y. Nabekawa, H. Hasegawa, E. J. Takahashi, and K. Midorikawa, Production of Doubly Charged Helium Ions by Two-Photon Absorption of an Intense Sub-10-fs Soft X-Ray Pulse at 42 eV Photon Energy, *Phys. Rev. Lett.* **94** 043001 (2005).

[19] P. Antoine, E. Foumouo, B. Piraux, T. Shimizu, H. Hasegawa, Y. Nabekawa, and K. Midorikawa, Two-photon double ionization of helium: An experimental lower bound of the total cross section, *Phys. Rev. A* **78** 023415 (2008).

[20] A. A. Sorokin, M. Wellhöfer, S. V. Bobashev, K. Tiedtke, and M. Richter, X-ray-laser interaction with matter and the role of multiphoton ionization: Free-electron-laser studies on neon and helium, *Phys. Rev. A* **75** 051402(R) (2007).

[21] A. Rudenko, L. Foucar, M. Kurka, Th. Ergler, K. U. Kühn, Y. H. Jiang, A. Voitkiv, B. Najjari, A. Kheifets, S. Lüdemann, T. Haermeier, M. Smolarski, S. Schüssler, K. Cole, M. Schöffler, R. Dörner, S. Düsterer, W. Li, B. Keitel, R. Treusch, M. Gensch, C. D. Schröter, R. Moshammer, and J. Ullrich, Recoil-Ion Momentum Distributions for Two-Photon Double Ionization of He and Ne by 44 eV Free-Electron Laser Radiation, *Phys.Rev.Lett.* **101** 073003 (2008).

[22] M. Kurka *et al*, Differential cross sections for non-sequential double ionization of He by 52 eV photons from the Free Electron Laser in Hamburg, FLASH , *New J. Phys.* **12** 073035 (2010).

[23] Z. Zhang, L. Y. Peng, M. H. Xu, A. F. Starace, T. Morishita and Q. H. Gong, Two-photon double ionization of helium: Evolution of the joint angular distribution with photon energy and two-electron energy sharing, *Phys.Rev. A* **84** 043409 (2011).

[24] Z. Zhang, L. Y. Peng, Q. H. Gong and T. Morishita, Momentum space analysis of multiphoton double ionization of helium by intense attosecond xuv pulses, *Optics Express* **18** 8976 (2010).

[25] J. S. Parker, L. R. Moore, K. J. Meharg, D. Dundas and K. T. Taylor, Double-electron above threshold ionization of helium, *J. Phys. B* **34** L69 (2001).

[26] B. Zhang, J. Yuan and Z. Zhao, DMTDHF: A full dimensional time-dependent HartreeCFock program for diatomic molecules in strong laser fields, *Comput. Phys. Commun.* **194** 84-96 (2015).

[27] J.C. Thibault and I. Senocak, CUDA implementation of a Navier-Stokes solver on multi-GPU desktop platforms for incompressible flows, in: Proceedings of the 47th AIAA Aerospace Sciences Meeting, Orlando, Florida, USA, 2009.

[28] NVIDIA CUDA ZONE.

https://developer.nvidia.com/cuda-zone. version 4.0, 2011.

[29] Y. Komura, OpenACC programs of the Swendsen-Wang multi-cluster spin flip algorithm, *Comput. Phys. Commun.* **197** 298 (2015).

[30] J.E. Stone, J.C. Phillips, P.L. Freddolino, D.J. Hardy, L.G. Trabuco, K. Schulten, Accelerating molecular modeling applications with graphics processors, *J. Comput. Chem.* **28** (2007) 2618.

[31] W. L. Cheng, A. Sheharyar, R. Sadr and O. Bouhali, Application of GPU processing for Brownian particle simulation, *Comput. Phys. Commun.* **182** 39 (2015).

[32] C. Broin and L.A.A. Nikolopoulos, A GPGPU based program to solve the TDSE in intense laser fields through the finite difference approach, *Comput. Phys. Commun.* **184** (2014) 1791.

[33] T. D. Nguyen, GPU-accelerated Tersoff potentials for massively parallel Molecular Dynamics simulations, *Comput. Phys. Commun.* **212** 113 (2017).

[34] L. Exl, A GPU accelerated and error-controlled solver for the unbounded Poisson equation in three dimensions, *Comput. Phys. Commun.* **221** 352 (2017).

[35] OpenACC official website. <http://www.openacc-standard.org/>.

[36] M. Venuti and P. Decleva, Convergent multichannel continuum states by a general configuration interaction expansion in a B-spline basis: application to H- photodetachment, *J. Phys. B* **30** 4839 (1997).

[37] R. Nepstad, T. Birkeland and M. Førre, Numerical study of two-photon ionization of helium using an ab initio numerical framework, *Phys. Rev. A* **81** 063402 (2010).

[38] R. Hasbani, E. Cormier and H. Bachau, Resonant and non-resonant ionization of helium by XUV ultrashort and intense laser pulses, *J. Phys. B* **33** 2101 (2000).

[39] H. Bachau, E. Cormier, P. Decleva, J. E. Hansen and F. Martín, Applications of B-splines in atomic and molecular physics, *Rep. Prog. Phys.* **64** 1815 (2001).

[40] Xi Zhao, Hui Wei, Yan Wu and C. D. Lin, Phase-retrieval algorithm for the characterization of broadband single attosecond pulses, *Phys. Rev. A* **95** 043407 (2016).

[41] Xi Zhao, Hui Wei, Changli Wei and C D Lin, A new method for accurate retrieval of atomic dipole phase or photoionization group delay in attosecond photoelectron streaking experiments, *J. Opt.* **19** 114009 (2017).

[42] T. Y. Shi, C. G. Bao and B.W. Li, Energy Spectra of the Confined Atoms Obtained by Using B-Splines, *Commun. Theor. Phys.* **35** 195(2001).

[43] Z. Zhang 2012, Two-photon double ionization of helium by solving full-dimentional TDSE Ph. D. Dissertation (Beijing: Peking University).

[44] A. Scrinzi and B. Piraux, Two-electron atoms in short intense laser pulses, *Phys. Rev. A* **58** 1310 (1998).

[45] W. Yu, X. Zhao, H. Wei, S.J. Wang, and C. D. Lin, Method for spectral phase retrieval of single attosecond pulses utilizing the autocorrelation of photoelectron streaking spectra, *Phys. Rev. A* **99** 033403 (2019).

[46] C. Wei and X. Zhao, Validity of extracting photoionization time delay from the first moment of streaking spectrogram, *Chin. Phys. B* **28** 013201 (2019).

[47] X. Zhao, H. Wei, W. Yu and C. D. Lin, Reconstruction of the complex angle-dependent photoionization transition dipole from a laser-dressed streaking experiment, *Phys. Rev. A* **98** 053404 (2018).

[48] L. F. Shampine and M. K. Gordon Computer Solution of Ordinary Differential equations: The Initial Value Problem (San Francisco, CA: Freeman) (1975).

[49] H. Li, V. A. Sautenkov, Y. V. Rostovtsev, M. M. Kash, P. M. Anisimov, G. R. Welch, and M. O. Scully, Carrier-Envelope Phase Effect on Atomic Excitation by Few-Cycle rf Pulses, *Phys. Rev. Lett.* **104** 103001 (2010).

[50] X. Zhao, J. Chen, P. Fu, X. Liu, Z. Yan, and B. Wang, Carrier-envelope-phase effect in a long laser pulse with tens of optical cycles, *Phys. Rev. A* **87** 043411 (2013).

[51] X. Zhao, Y. Yang, X. Liu and Bingbing Wang, Carrier Envelope Phase Effect of a Long Duration Pulse in the Low Frequency Region, *Chin. Phys. Lett.* **31** 043202 (2014).

[52] Dian Peng, Biao Wu, Panming Fu, Bingbing Wang, Jiangbin Gong and Zong-Chao Yan, Sensitive frequency dependence of the carrier-envelope phase effect on bound-bound transitions: An interference perspective, *Phys. Rev. A* **82** 053407 (2010).

[53] T. Nakajima and S. Watanabe, Effects of the Carrier-Envelope Phase in the Multiphoton Ionization Regime, *Phys. Rev. Lett.* **96** 213001 (2006).

[54] Z. Zhai, D. Peng, X. Zhao, F. Guo, Y. Yang, P. Fu, J. Chen, Z. Yan, and B. Wang, Carrier-envelope-phase effect on laser-driven bound-bound transitions in the high-frequency region, *Phys. Rev. A* **86** 043432 (2012).

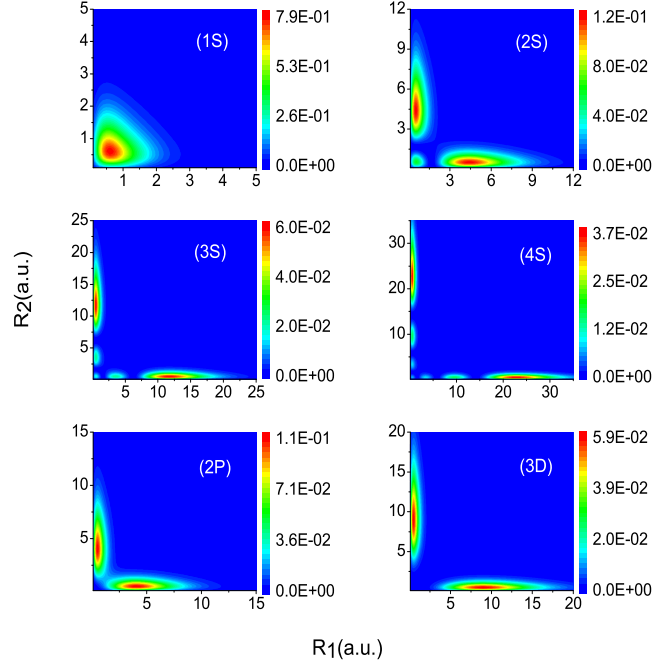


FIG. 1: (Color online) The density distributions of some bound states in coordinate space.

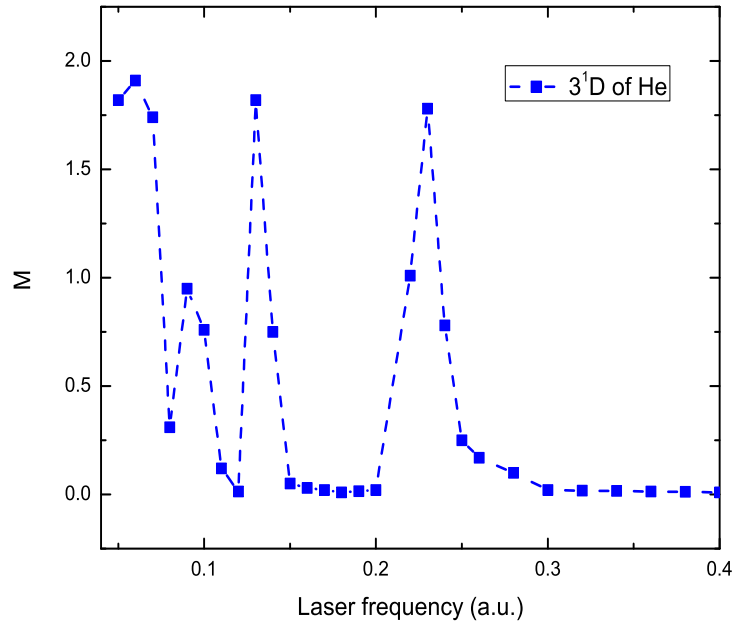


FIG. 2: (Color online) The CEP parameter M vs the laser frequency for 3^1D state of helium.

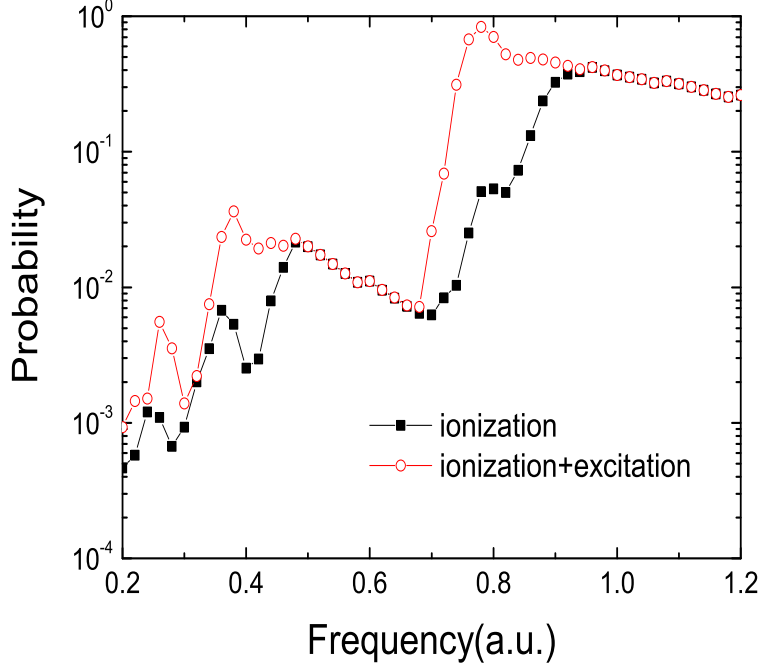


FIG. 3: (Color online) Excitation and ionization probabilities, for the helium atom, with a pulse duration of 3.8 fs (fixed) and a peak intensity of $2.96 \times 10^{14} W/cm^2$.

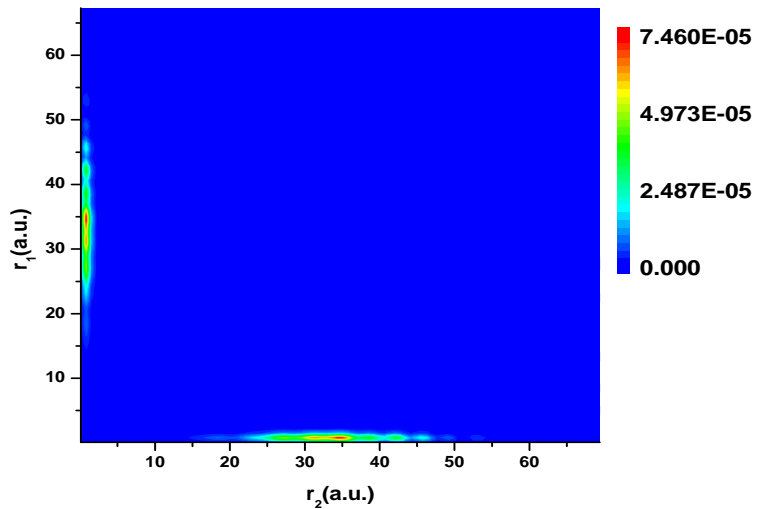


FIG. 4: (Color online) The distributions of the continuum state in the coordinate space $\omega = 1.0$, FWHM=2 OC, intensity $I = 1.0 \times 10^{13} W/cm^2$ when the laser is end.

TABLE I: The energy level of some bound states.

Helium states	Our results	Ref. [44]	Ref. [23]	Ref. [43]
1^1S	-2.900029	-2.903531	-2.903669	-2.903724
2^1S	-2.145044	-2.145961	-2.145970	-2.145974
3^1S	-2.060512	-2.061268	-2.061271	-2.061272
4^1S	-2.032866	-2.033585	-2.033585	-2.033587
2^1P	-2.123121	-2.123832	-2.123839	-2.123843
3^1P	-2.054443	-2.055143	none	none
3^1D	-2.054927	-2.055621	-2.055555	-2.055620
4^1D	-2.030586	-2.031280	none	none
4^1F	-2.030562	-2.031255	none	none
5^1F	-2.019272	-2.020003	none	none

TABLE II: The efficiency of our GPU program.

Basis number	GPU time	CPU time	Speed-up ratio
3000	41.22	3644.07	88.41
3600	48.61	4963.76	102.11
4200	60.06	7278.36	121.18
4800	86.26	12625.83	146.37